Thermal conductivity and characterization of compacted, granular silica aerogel

Citation: Neugebauera, A., K. Chen, A. Tang, A. Allgeier, L.R. Glicksman, and L.J. Gibson. "Thermal conductivity and characterization of compacted, granular silica aerogel." Energy and Buildings 79 (August 2014), pp. 47-57.

As Published: http://dx.doi.org/10.1016/j.enbuild.2014.04.025

Publisher: Elsevier

Persistent URL: http://hdl.handle.net/1721.1/103951

Version: Author's final manuscript: final author's manuscript post peer review, without publisher's formatting or copy editing

Thermal Conductivity and Characterization of Compacted, Granular Silica Aerogel

Neugebauer A[1], Chen K[2], Tang A[3], Allgeier A[4], Glicksman LR[1] and Gibson LJ[3]

NOTE: Need to verify that similar author order and formatting is used on the cover page of the submittal.

[1]Department of Architecture
[2]Department of Mechanical Engineering
[3]Department of Materials Science and Engineering
Massachusetts Institute of Technology
Cambridge, MA 02139

[4]Central Research Department
DuPont Experimental Station
Wilmington, DE 19881

Corresponding Author

Lorna J. Gibson
1-617-253-7107
ljgibson@mit.edu

77 Massachusetts Avenue
Building 8, Room 135
Cambridge, MA 02139

Abstract

Monolithic silica aerogels are well known for their low thermal conductivity (approximately 15 mW/(m K)) [3]. Their low relative density (typically less than 5%) reduces conduction through the solid and their small pore size, typically less than one hundred nanometers, on the order of the mean free path of air, reduces conduction through air, as well as convection and radiation. As they are fragile and brittle, they are often used in a granular form in thermal insulation, with some increase in their thermal conductivity from the air between the granules. Here, we describe a technique for compacting a bed of granular silica aerogel that reduces the thermal conductivity from 24 mW/(m K) (when uncompacted) to 13 mW/(m K) (after compaction). We find that there is an optimum level of compaction to minimize the thermal conductivity: at higher levels of compaction, the contact area between the granules increases and the granules densify, increasing conduction through the solid.

Keywords

Strain measurement; tomography; cellular materials; porous materials; fracture

Introduction

With the ever-increasing importance of energy efficiency, improved products and techniques for thermal insulation are needed. Aerogels are one such cutting-edge material with significant potential to meet this need. [1, 2] Their thermal conductivities are typically around 15 mW/(m K) [3], much lower than that of conventional insulations, such as standard fiberglass batts (40 mW/(m K) [4]) and closed-cell polyurethane foams (25 mW/(m K) [5]). After cost, one of the main limitations that has prevented aerogels from becoming more widely used as a high-performance insulation product is their fragility, which results from their low density and inefficient distribution of solid for resisting mechanical loads.

The solid matrix of the nanoporous microstructure of aerogels can be described as "beads on a string" or "pearls on a necklace" [3], referring to their structure of roughly spherical particles connected by small necks or thin strands. For a given mass of material, this structure is much less stiff and strong than that of an open-cell foam (or a fully dense solid). For instance, at a density of 100 kg/m^3, the modulus and flexural strength of silica aerogels are typically 1 MPa and 0.02 MPa, respectively [6]; by comparison, rigid, closed-cell polyurethane foams of similar density have moduli and strengths of about 10 MPa and 0.6 MPa, respectively [5]. The Young's modulus and strength of aerogels decreases with decreasing density much faster than those of open-cell foams: the Young's modulus of aerogels varies with relative density raised to the power 3.7 [6] while that of open-cell foams varies with relative density squared [5]; and the flexural strength of aerogels varies with relative density raised to a power of between 2.5 and 3 [6, 7] while that of open-cell foams varies with relative density raised to the power 1.5 [5]. (Relative

density is the density of the porous material divided by that of the solid from which it is made.).

The microstructure of aerogels also gives rise to their extremely low thermal conductivities [8]. Heat transfers from one object, surface or substance to another in three main ways: by conduction, convection and radiation [9]. Conduction is minimized by reducing the volume fraction of solid in the material (as solids have higher thermal conductivities than gases), which is why most insulations have relatively low densities. The remainder of the insulation is filled with a gas, such as air (thermal conductivity of 25 mW/(m K)), but which is susceptible to convection and radiation. With large voids, these two mechanisms can provide much higher heat transfer than solid conduction. Large voids allow radiation to quickly bypass significant lengths of the material and convection currents to be set up. Therefore, to minimize these heat transfer modes, the air (or gas) is typically contained in small pockets throughout the material; this is why most insulation materials are designed to have small pore sizes. In closed-cell foams with pore sizes less than a few millimeters, convection is negligible, as the buoyancy forces associated with a temperature gradient across the cell are countered by viscous drag of the fluid against the walls of the foam. In aerogels, the pores are at the scale of 2 to 50 nm [10], less than the mean free path of air, significantly reducing conduction through the gas, too. Insulation materials can also decrease heat transfer by replacing the air within the pores with a lower conductivity gas (such as argon) or by decreasing the air pressure inside the insulation (as in vacuum insulated panels).

As a result of their fragility, silica aerogels used in commercial products are often in a granular form, so that handling the material becomes easier and varying shapes of

cavities can be more readily filled. However, since there is air in the interstitial spaces between the silica aerogel granules and the thermal conductivity of air is higher than that of monolithic aerogel (25 mW/(m K) for air versus typically 15 mW/(m K) for silica aerogel at ambient conditions [3]), a bed of granular aerogel has a higher thermal conductivity than monolithic aerogel. Here, we describe and characterize a means of compacting silica aerogel granules, reducing the interstitial volume fraction of air and decreasing the thermal conductivity of the granular bed from 24 mW/(m K) (when uncompacted) to 13 mW/(m K) (after compaction), almost a 50% reduction in thermal conductivity. In a companion paper [11], we describe the use of compacted granular aerogels in a sandwich panel with a three-dimensional truss core, which combines structural support with low thermal conductivity, suitable for building applications; the panel, which is opaque, is intended for insulation of walls rather than fenestration.

Materials and Methods

The granular silica aerogel used in this study was commercially available Cabot P100 aerogel (Cabot Corporation, Billerica MA). According to Cabot literature and correspondence with a Cabot representative, the thermal conductivity of an "untapped" particle bed of this material at room temperature was about 22 mW/(m K) and the density of individual particles ranged from 120 to 180 kg/m^3 [12, 13]. The bulk granular aerogel was uniaxially compressed in modified graduated cylinders. The microstructure of the as-received and compacted granular aerogel was characterized by micro-computed tomography imaging, as well as measurement of the particle size distribution by sieving, and the pore size distribution and internal surface area by gas absorption/desorption

analysis, described in more detail below. The volume fraction of air in the interstitial spaces between the particles was calculated. The thermal conductivity was measured on bulk samples of the as-received and compacted granular aerogel.

Compaction Technique

Since air has a higher thermal conductivity than monolithic aerogel, the conductivity of a bed of aerogel granules can be reduced by decreasing the volume of air in the interstitial spaces between the granules. In this study, we achieved this by compacting the granules together in a cylindrical mold.

The initial naturally-settled bed (or bulk) density of the Cabot aerogel was approximately 68 kg/m^3. The compression percentages mentioned in this research reference the compaction from this initial bed density. These percentages and their approximate corresponding bed densities can be found in Table 1. Compaction was performed in modified graduated syringes marked in 1 mL increments, since they provided a convenient means of tracking the changes in height and volume of the samples during the experiment. A flat plastic base was inserted into the bottom of the cylinder of the syringe to prevent granules from exiting through the hole at the tip of the syringe. The volumetric scale of the syringe was consequently offset by the thickness of this base. A flat base was also attached to the end of the plunger, such that a cylindrical chamber was formed to hold the granules. These bases were designed to fit loosely enough in the syringe such that the granules are maintained but air is free to move in and out of the sample column. An Instron mechanical testing machine (Model 4201, Instron, Canton,

MA) was used to compact the granules to strains ranging from 10% to 70% at a nominal compaction speed of 10 mm/minute.

Micro-Computed Tomography

Micro-computed tomography (micro-CT) uses x-rays to scan a three dimensional object and a computer to process the data from the scan to allow users to see cross sections of solid objects. Aerogel granules were first compressed in modified cylindrical chambers to different bed densities, and then scanned with a micro-CT scanner at the David H. Koch Institute for Integrative Cancer Research at MIT (GE eXplore CT 120, 25 micron resolution; Little Chalfont, UK). These scans provided a three-dimensional digital image of the sample which could be viewed, slice by slice, in planar cross sections in a grayscale format. Objects that appeared in a lighter shade of gray corresponded to a higher density, while darker shades of gray represented lower density materials. Due to the similarity in density, and consequently in the gray color between the aerogel granules and the ambient air, it was difficult to distinguish between the granules and the interstitial air in the initial scans. To improve the contrast between the granules and the interstitial spaces, the samples were submerged and compressed in water. During compression the water was free to flow out of the cylindrical chamber through a filtered opening, to minimize any additional stresses from the water pressure, and to keep the hydrophobic granules in the chamber. One sample with an initial uncompressed granular volume of 20 mL was scanned at each level of compression. Images of the compressed granules in air and in water are shown in Fig. 1.

Determining the Grayscale Threshold and the Volume Fraction of Air

The digital planar cross sections obtained by the scanner were then analyzed using ImageJ, an image-processing program developed at the National Institutes of Health. A histogram of the grayscale level of all voxels in a sample was first plotted (Fig. 2). By specifying an appropriate grayscale threshold value, the granules were identified, allowing the volume fraction of air to be computed at each compression level. The grayscale threshold that optimally distinguishes the aerogel granules from the interstitial water between the granules corresponds to the deepest part of the trough between the peak for each phase in the grayscale histogram [14]. For the lower compaction strains (0-20%), this method was effective since a trough was clearly discernible in the grayscale histogram. However, at higher compression levels, the trough became less clear as the volume fraction of water decreased and there were fewer pixels with grayscale values corresponding to water in the histogram, decreasing the size and height of peak of the bell curve corresponding to the water in the histogram. As a result, the grayscale thresholds for the higher compression samples had to be identified in a more visual and qualitative manner. ImageJ has a tool which allows users to highlight all pixels with a grayscale less than a chosen threshold value. Using this feature, a user can manipulate the grayscale threshold value until all the aerogel granules are highlighted, thereby finding a nominal threshold value.

Once a grayscale threshold value is chosen, ImageJ can filter the captured images to be binary. In other words, every voxel under the grayscale threshold is given value of 1, and everything above the grayscale threshold is given a value of 0. Using a supplementary voxel counter program, ImageJ can then count the instances of 0 and 1

valued voxels in the sample and deduce the volume fraction of the material of interest. By assigning a voxel value of 1 to all aerogel particles under a specified grayscale threshold and a voxel value of 0 to all the scanned water and using the voxel counter, the volume fraction of aerogel was calculated, consequently giving the volume fraction of the pores between the granules as well.

Particle Size Distributions

The particle size distribution of samples compressed to different strains was measured by passing each sample through a tower of sieves with progressively decreasing mesh sizes at lower levels; the tower was agitated by a motorized sieve shaker at a constant speed to facilitate the flow of granules. When the flow of granules stopped, the mass of aerogel in each sieve was measured to give the particle size distribution. Four specimens were analyzed at each compression level. Average values, with error bars indicating the standard deviation of the samples, are reported. Each sample contained 140 mL of naturally settled aerogel particles, to ensure a sufficient number of particles for statistical relevance. Any potential coalescing of the granules in compression is assumed to be negated by the agitation process.

Nanopore Size Distribution within the Granules

The small pore size of the silica aerogel, on the order of the mean free path of air, reduces heat transfer by conduction through the air and by radiation, and virtually eliminates convection, giving rise to aerogel's exceptional insulating properties. By physically compressing the aerogel granules, there is a possibility that the nanoporous

structure was compromised. Compressed granular samples were subjected to a gas adsorption/desorption analysis, with supplementary data reduction methods to determine the pore size distribution within the granules, as well as the surface area and pore volume.

The gas adsorption technique begins with placing the sample in a tube and heating it to 100ºC under vacuum for 12 hours. This ensures that any preexisting adsorbates such as water and other unwanted contaminants are released from the pores of the sample. The sample then undergoes porosimetry analysis, in which the tube is again evacuated and cooled in liquid nitrogen. The analysis gas (nitrogen) is then dosed into the tube in small increments of pressure, up to 101 kPa. This constitutes the adsorption stage of the procedure where the gas fills the pores of the tested material. As the pressure rises more nitrogen molecules accumulate on the surface of the sample until all pores in the sample are saturated and the nitrogen liquefies. The pressure in the system is then slowly decreased and the condensed nitrogen evaporates from the pore, constituting the desorption phase of the analysis. From the collected isotherm data the Brunauer, Emmett and Teller method (BET method) can be used to calculate the surface area of the sample. Simultaneously, a calculation developed by Barrett, Joyner and Halenda (BJH method) can also be implemented to obtain data on the pore size distribution [15, 16]. Holes with a diameter of 0.38 mm were drilled into the syringes to facilitate gas diffusion into the granular sample and temperature equilibrium during the experiment. Four holes were drilled approximately 1 cm apart along the length of the syringe, through the entire thickness of the syringe. Preliminary samples were tested repeatedly and yielded consistent results to verify that the structural integrity of the aerogel granules was not compromised from the test methodology. Two sets of samples were tested: in the first set,

one sample at each compression level was tested three times and in the second set, three samples were tested once at each compression level.

Hot-Wire Thermal Conductivity Characterization

A test chamber (Fig. 3a) was constructed to allow hot-wire thermal conductivity testing of granular materials under uniaxial compression. Our tests included a number of small monolithic samples as well as granules under different compression levels and in a vacuum chamber. Our research team ultimately determined that the hot-wire test method [17] was the best method to obtain comparable results. In the sandwich panel paper [11], hot-plate tests were performed for comparison purposes using a rigid sandwich panel system; the thermal conductivities for aerogel granules at the same bed density observed by the hot-wire and hot-plate tests were within 2 mW/(m K) of each other. Similar experiments have been reported measuring the thermal conductivity of compressed beds of silica aerogel granules as a function of external load using a hot-plate apparatus [18, 19].

The internal dimensions of the hot-wire test chamber were 9.0 by 5.0 by 7.5 cm (length by width by height) and the hot-wires were installed to lengths between 7 and 8 cm. The 25.4 μm diameter platinum hot-wire was suspended through the lower half of the chamber, which was then filled with aerogel granules to surround the wire. A steady electrical current, of 65 amps, was run through the wire for a short duration (1.0 sec in our tests). This created resistance heating in the platinum wire. This heat either dissipates through the surrounding material or causes the temperature of the wire to increase. The lower the thermal conductivity of the surrounding material, the greater the

temperature increase in the wire. Therefore, by measuring the temperature increase in the hot-wire, one can determine the thermal conductivity of the surrounding material.

A compression plate was used to bring the internal volume of the chamber to the desired level. The mass of the granules poured into the chamber was measured along with the internal volume of the chamber (based on the height of the compression plate) in order to calculate the bed density and corresponding compression strain of the granules. The plate was used to incrementally compress the granules after each set of hot-wire tests in order to measure the thermal conductivity of the aerogel granules across a range of compression levels.

Initial hot-wire tests, conducted previously in our group, indicated that the measured conductivity depended on the length of the hot-wire, as a result of the platinum wire being soldered to a much larger copper lead, which acted as a heat sink. Our group developed an analytical method to correct for this effect, which successfully removes the dependence of the measured conductivity on the length of the wire [20].

Due to the transient nature of the hot-wire test and the relatively high infrared transmissivity of the aerogel, this test method underestimates the contribution of radiation to the overall heat transfer through the aerogel granules when compared to the steady-state hot-plate method. While the hot-plate method is more representative of the conditions the product would be subject to in the field, these systems are not designed to handle granular materials. The magnitude of this underestimation was previously estimated – using the optically thick Rosseland approximation – to be up to 3.3 mW/(m K) based on laboratory measurements of the transmissivity and extinction coefficient of monolithic aerogel versus wavelength [20]. Since the exact magnitude of this

underestimation is not currently known, the hot-wire results expressed in this paper have not been adjusted to account for this underestimation.

Additionally, it had been previously shown that the thermal conductivity of monolithic aerogel samples can be significantly reduced with even modest levels of vacuum. However, granular samples had only undergone minimal testing in the vacuum [20]. Therefore a vacuum chamber was obtained in order to repeat the hot-wire tests across a range of bed densities with increasing levels of depressurization. Due to the internal dimensions of the vacuum chamber, a smaller test chamber was developed. The original test chamber design was modified to maximize its internal dimensions within the constraints of the vacuum chamber. The new test chamber had internal dimensions of 5.4 by 2.6 by 4.5 cm (length by width by height) and the hot-wires were installed to lengths between 3 and 4 cm. During the test, the leads from the test chamber were connected to wires that led through the chamber stem to a multi-pin port on the outside of the vacuum chamber. The chamber was depressurized with a rotary vane vacuum pump until the internal pressure was at or below the desired pressure, at which point the supply valve was closed and the vacuum pump was turned off. The internal pressure was fine-tuned with the release valve as needed (Fig. 3b). Note that the pressure gauge was installed at a T-junction along the supply tube for the vacuum chamber. Measuring the air pressure directly within the test chamber was not feasible for these tests.

Results

Sample Compaction and Rebound

Compaction in the aerogel granules was achieved by the uniaxial compression method. When the compressive load is removed from the granular aerogels, however, the sample rebounds, such that not all of the compressive strain is maintained in the sample. The granules do not fully return to the initial uncompressed state, but creep and expand out from the target compression level. Consequently, the effect of different methods of compression on specimen rebound was explored. All samples had an initial uncompressed bulk volume of 20 mL. Samples were compressed by holding each at the maximum compressive strain for varying times or by repeated compaction. The volumetric rebound was measured using the markings on the modified graduated syringes. Two specimens were tested for each type of time-based compression method.

For samples held under compression for different durations of time, the longer they were held, the more slowly and less the samples rebounded from the target compaction level. Given sufficient time to freely expand and settle, the final rebound strains approximately converge, as seen in Fig. 4, so that specimens that were compressed for 5 hours and for 3 days both rebounded by slightly over 25% after they were unloaded for one hour.

The aerogel granules were also cyclically compressed at a rate of 10 mm/minute to determine if the amount of spring-back on release could be reduced. A single specimen was tested for each regime of cyclic compression. Fig. 5 shows that indeed the particles rebounded less as the number of compression cycles increased. The rebound generally begins to plateau after 10 cycles. Samples at higher target compaction levels demonstrate a higher benefit in rebound percentage as a function of cycling. Furthermore,

the ratio of rebound volume to compressed volume seems to reach a constant value once compression reaches and exceeds 30%.

Micro-Computed Tomography Imaging and Volume Fraction of Air

Micro-CT images of cross sections of increasingly compressed specimens (from 0 to 60%) are shown in Fig. 6. The micro-CT scans at 60% compression show granules that appear to be very tightly packed, and the distinct particulate features of the granules visible at lower degrees of compression is difficult to discern. The scans also visually depict a slightly greater compaction near the top of the sample column, possibly due to higher localized forces associated with frictional effects due to the proximity of the compressing syringe plunger. The volume fraction of interstitial air between the granules is reduced from 45% in the uncompressed samples to 2.5% in the samples compressed to 60% strain (Fig. 7a).

The densities of the granules were calculated using the bed densities and the volume fraction of air (Fig. 7b). The calculated values of the densities of the granules are relatively consistent for compressive strains between 0 and 40%, at about 110-120 kg/m^3, and increase to 174 kg/m^3 at a compression of 60%.

Particle Size Distribution

The particle size distributions of samples compressed to 10, 40 and 70% are shown in Fig. 8. Distributions for other compression strains fell between these values in a systematic way; they are omitted for clarity. As the degree of compaction increases, the fraction of smaller granules increases. This is expected since higher degrees of

compaction require a greater amount of force to achieve, and a higher probability of larger granules becoming broken down into smaller ones.

Samples that were compressed multiple times showed possible signs of pulverization, characterized by a white and powder-like quality in the granular sample. The particle size distribution of specimens subjected to cyclic compression was also measured. Four, 140 mL samples were compressed to 50% once, five times and ten times. Fig. 9 shows the averaged distribution results of these measurements. Among the different samples plotted, the distributions are fairly consistent and reside within the standard deviations of one another. This suggests a negligible effect of the number of compressive cycles (up to ten) on the aerogel particle size distribution up to 50% compression.

Nanopore Size Distribution within the Granules

The gas adsorption analyses gives data for the pore size distribution, surface area and pore volume within the granules, on uncompacted samples and samples compacted to 20, 40, 50, 60 and 70% compression. Typical adsorption/desorption isotherms for the different levels of compression are shown in Fig. 10a. The curves are consistent among the samples, and demonstrate a Type IV physisorption isotherm, according to the International Union of Pure and Applied Chemistry (IUPAC) classification system [21]. This isotherm type is characterized by the prominent hysteresis loop, which is consistent with“ink-bottle” pores in the material, comprising a narrow neck at the surface of the material which expands into a wider body [22]. The peak value of the isotherms remains constant for compression strains between 0 and 50% but decreases for 60 and 70%

compression strain, indicating that the maximum quantity of nitrogen adsorbed by the aerogel, and the total pore volume, decreases at the two highest compression strains. Other notable differences in the isotherms can be seen in the hysteresis loops of samples compressed past 60% strain: first, a slightly reduced hysteresis loop and second, the point on the adsorption curve at which the slope of the curve rises dramatically is at a lower pressure compared to lower compression levels (Fig. 10b).

The pore width measurement from the adsorption/desorption isotherms corresponds to the "neck" of the ink-bottle. 98% of the pores within the granules are smaller than the mean free path of air (66 nm [23], Fig. 10c). One sample at 20% compression, one sample at 40% compression and one sample at 70% compression were each tested three times to determine the variability of the data; the maximum coefficient of variation was 0.047 (Fig. 10d). More extensive results, on three specimens at each level of compression, are shown in Fig. 10e: with increasing compression, the average pore width was roughly constant; the surface area had no discernible trend and the pore volume decreased at the highest level of compression.

Thermal Conductivity as a Function of Compression Strain

The thermal conductivity data at ambient air pressures are shown in Fig. 11. The hot-wire system was calibrated with a low-conductivity standard reference material (SRM 1459) from the National Institute of Standards and Technology, which was measured within 5% of the stated conductivity; however, an unknown portion of this disagreement can be attributed to the anisotropic nature of the reference material. In general, the uncertainty of the hot-wire methodology can be less than 1% [17]. Based on the accuracy of the bed volume and granule mass measurements, it was estimated that

uncertainty in the bed density measurements was less than 10%. The data demonstrate that the thermal conductivity initially decreases as the granular bed density increases, reaching a minimum value of 13 mW/(m K) at a bed density of about 150-165 kg/m^3, or a compressive strain between 55 and 59%. At higher bed densities, the thermal conductivity appears to begin to gradually increase. The hot-wire thermal conductivity tests were also performed on a high-performance silica aerogel based on a formulation previously developed at Massachusetts Institute of Technology [24]. The MIT samples were synthesized using a super-critical drying process (compared to an ambient drying process for the Cabot granules [25]) and then granularized manually. Both MIT and Cabot granules showed similar compression-conductivity responses, though the MIT samples appeared to achieve similar thermal conductivities to the Cabot samples at lower bed densities. We were unable to determine the minimum conductivity point of the MIT samples because the fragile platinum wire broke on each test before this point was reached; however, the lowest recorded conductivity for the MIT samples (about 12 mW/(m K)) was lower than the absolute minimum found with the Cabot samples.

The thermal conductivity data across a range of air pressures are shown in Fig. 12. The pressure gauge measurements were accurate to within 10% for the range of pressures measured, according to product documentation [26]. Additionally, the pressure measurements were taken outside of the aerogel bed (see Fig. 3b), though the impact this might have on these measurements could not be readily quantified. Results from previous testing of a monolithic MIT sample have also been included for comparison [20]. The MIT and Cabot granules demonstrated similar patterns in their thermal conductivity versus air pressure curves. They all showed the overall trend of having lower

conductivities at lower air pressures, since a vacuum has a lower conductivity than air. Also, below 1 kPa it appeared that the thermal conductivities began to converge for different bed densities. This limit likely represents the pressure at which the mean free path of the air in the intergranular voids is approximately equal to the void dimensions.

Discussion

The thermal conductivity of compacted granular aerogel from Cabot decreases from roughly 24 mW/(m K), for the uncompacted granules, to a minimum of about 13 mW/(m K), for granules compressed to a strain of 55-59% (or a bed density of 150-165 kg/m^3, similar to that of a monolithic aerogel [12]). Further compaction increases the conductivity slightly. The reduction in thermal conductivity is associated with the reduction in the volume fraction of interstitial air between the granules, which drops from 45% in the uncompressed samples to 2.5% at 60% strain (Fig. 6, 7a). At high strains, the microstructure within the granules begins to collapse, increasing conduction through the solid. Analysis of the micro-CT images suggests that densification of the granules begins at a compressive strain of about 50% (Fig. 7b). The adsorption/desorption data indicate that while there is some decrease in the pore volume within the granules (and thus densification) at a compressive strain of 50%, densification becomes pronounced at a compressive strain of 70% (Fig. 10e).

Consideration of the "ink-bottle" shaped pores and the results of the adsorption/desorption analyses offer further insight into the increase in thermal conductivity at higher compressive strains. The pore volume decreases at higher levels of compression, while the pore width remains constant (Fig. 10d, e). This suggests that

while the narrow opening of the pores (the "neck" of the "ink-bottle") is unchanged, the compressive forces are shrinking or collapsing the wider bodies of the pores (the "well" of the "ink-bottle") at the higher levels of compression. This is further demonstrated in a comparison of the isotherms for 0, 40 and 70% compression in Fig. 10b. The desorption phase of the plot is strictly indicative of the pore openings, as this is the only factor that affects the nitrogen evaporation rate. There is no clear trend among the samples in this phase. The adsorption stage describes both the pore opening and body, as gas incrementally accumulates layer by layer along the pore walls. The point on the adsorption curve at which the slope of the curve rises dramatically indicates the pressure at which nitrogen begins to rapidly condense in the sample. This point occurs at a higher pressure for the 0 and 40% compressed granules compared to the 70% compressed granules; more pressure is needed to force the nitrogen to condense in the pores of the less compressed samples. This suggests the presence of wider pore bodies in the less compressed samples, which inherently require more pressure to liquefy the nitrogen gas inside the pore. At compression strains beyond 60%, this critical pressure decreases, suggesting that the pore bodies decrease in size and the granules densify, leading to increased conduction through the solid.

The MIT aerogel granules exhibit a similar compression-conductivity relationship as the Cabot granules, though the MIT aerogel showed a lower thermal conductivity for a given compressive strain or bed density. According to the hot-wire results, the MIT granules achieved similar thermal conductivities as the Cabot granules at bed densities approximately 20-30 kg/m^3 lower than the Cabot granules. Also, the MIT granules approached a thermal conductivity of 12 mW/(m K) and did not appear to have yet

reached their minimum point; the minimum conductivity of the Cabot granules was about 13 mW/(m K).

When the hot-wire tests were repeated under vacuum, the granular aerogels decreased in conductivity at lower pressures. As the air pressure decreases, the mean free path of air increases. Once the mean free path is limited by the internal pore or intergranular void size, the thermal conductivity begins to drop. For monolithic aerogel samples (with pore sizes on the order of 2-50 nm), the mean free path of air will quickly be limited and therefore the thermal conductivity will drop quickly at even modest decreases in air pressure [20]. On the other hand, a bed of granules will contain relatively large inter-granular voids in additional to the nanopores within each granule. The granules themselves should behave similar to the monolithic samples, but the conductivity behavior of the intergranular voids will depend on their size and distribution. Based on the results from the granular samples, it appears that after an initial drop in conductivity, the slope of the curve for the thermal conductivity of the granular aerogel is decreased from 51 kPa until around 5 kPa, at which point conductivity begins dropping more steeply again. The initial drop in conductivity is most likely due to mean free path being limited by the nanopores within granules and the later drop is due to the mean free path finally being reached in the inter-granular voids. At higher bed densities, the plateau effect appeared less distinct (presumably due to a decrease in the size of the inter-granular voids) and the curve appeared to more closely resemble the shape obtained from the monolithic samples.

The rebound of the compressed aerogels led to the investigation of two different methods of compression: cyclic compression of the granules and holding the compression

strain for varying durations of time. Both approaches gave similar results (Fig. 4, 5). From the viewpoint of manufacturing, the cycling method is more appropriate, as it is more economical and can be achieved in the span of minutes compared to storing the granules under compression for hours or days.

There are several sources of error in our data. At compressive strains above 20%, the selection of the threshold for identifying the aerogel and water was somewhat subjective, as a distinct trough in the histogram of grayscale values was not apparent. The calculated volume fraction of interstitial air between the granules could vary somewhat, depending on the grayscale threshold value selected. Comparison of the measured values (Fig. 7a) with the micro-CT images (Fig. 6) suggests that the error is not large.

The specimens used for the adsorption/desorption tests were small, with a mass of approximately 0.065 grams each. The variability between the small specimens was characterized by repeating the adsorption/desorption test three times on one specimen (Fig. 10d) as well as obtaining data for three specimens, each tested once, at each compression level (Fig. 10e). The variability in the data, as characterized by the standard deviation normalized by the mean, was acceptable.

The adsorption/desorption isotherms are Type IV, indicating that the pores have an "ink-bottle" shape. The pore width measurements represent that of the "neck" of the ink-bottle, rather than the wider "body". The low thermal conductivity measurements suggest that the pore size of a typical "body" is still less than the mean free path of air.

Pulverization and granular fracturing were noted in the samples as they endured compression. This benefits the packing process as the smaller granules are more able to

fill the interstitial voids between larger particles, up to the limit at which the granules are crushed to the point of compromising the aerogel's microstructure and insulation properties. The thermal conductivities measured in this study could be decreased further with an improved packing methodology. Higher packing densities could potentially be achieved if the particles were subjected to mechanical agitation during compression. This would encourage particles to settle into voids more easily. The study could also be improved with samples with more regularly shaped particles.

Conclusions

Using the hot-wire test method, we were able to demonstrate that the thermal conductivity of granular aerogels can be reduced through compression and also through decreased air pressure. The former is due to the reduction in the volume of interstitial air-filled voids between the granules while the latter occurs when the conductivity of air (in the voids between granules and in the pores within granules) decreases at low enough pressures. In addition, we demonstrated that there is an optimum level of compression that minimizes the thermal conductivity. In our experiments with the Cabot granules, the minimum conductivity was reached at a bed density of 150 to 165 kg/m^3, or at a compressive strain of 55 to 59%. Our results suggest that the leveling off and subsequent small increase in conductivity at higher levels of compaction is due to increased conduction through the solid structure associated with a densification of the granules. Theoretically, one could expect that the absolute minimum one could achieve through compression of the bed of granules would be equal to the thermal conductivity of a monolithic sample; this would assume, however, that the compression eliminates

interstitial voids only, without altering the nanoporous structure, which is not realistic, and therefore this value represents a theoretical minimum. Also, at low levels of compressive strain, the conductivity decreases modestly with decreased air pressure until lower pressures are achieved (about 5 kPa); at higher compressive strains, the conductivity curve for granular aerogel looks more like the monolithic curves where significant decreases in conductivity can be achieved at moderate pressures (between 101 and 10 kPa).

The techniques described in this paper to improve the thermal conductivity of a bed of aerogel granules have applicability to any thermal insulation system that relies upon granular aerogel materials. In particular, insulation systems that could allow for sufficient control of the level of bed compaction during manufacture (such as sandwich panel systems or window units) could reliably obtain consistent reductions in thermal conductivity. Further research on this technique could focus on the impacts of particle size distribution and particle morphologies on the compression-conductivity relationship and on the impacts of bed compaction on the solar heat gain and light transmission values for fenestration applications.

Acknowledgements

We gratefully acknowledge the financial support provided by the DuPont-MIT Alliance and technical discussions with our DuPont liaison, Dr. Vivek Kapur. Milton Cornwall-Brady of the Koch Institute for Integrative Cancer Research supervised and assisted in the micro-CT scans of the aerogel samples. We would also like to thank Dr.

Jack Germaine for the loan of sieving equipment for the particle size distribution measurements.

References

[1] R. Baetens, B.P. Jelle, A. Gustavsen, Energy and Buildings 43 (2011) 761.

[2] T. Stahl, S. Brunner, M. Zimmermann, K. Ghazi Wakili, Energy and Buildings 44 (2012) 114.

[3] M.A. Aegerter, N. Leventis, M.M. Koebel, eds., Aerogels Handbook, 1st ed., Springer-Verlag New York, LLC, New York, NY, 2011.

[4] M.K. Kumaran, A Thermal and Moisture Transport Property Database for Common Building and Insulating Materials: 1018-RP□: Final Report for American Society of Heating, Refrigerating and Air-conditioning Engineers, National Research Council Canada, Ottawa, Ontario, 2002.

[5] L.J. Gibson, M.F. Ashby, Cellular Solids: Structure and Properties, 2nd ed., Cambridge University Press, Cambridge, 1997.

[6] T. Woignier, J. Reynes, A.H. Alaoui, I. Beurroies, J. Phalippou, Journal of Non-Crystalline Solids 241 (1998) 45.

[7] T. Woignier, J. Phalippou, Journal of Non-Crystalline Solids 100 (1988) 404.

[8] S.S. Kistler, A.G. Caldwell, Industrial and Engineering Chemistry 26 (1933) 658.

[9] Y.A. Çengel, Heat and Mass Transfer, 3rd ed., McGraw-Hill, New York, NY, 2007.

[10] A. Soleimani Dorcheh, M.H. Abbasi, Journal of Materials Processing Technology 199 (2008) 10.

[11] K. Chen, A. Neugebauer, T. Goutierre, A. Tang, L.R. Glicksman, L.J. Gibson, Mechanical and Thermal Performance of Aerogel-Filled Sandwhich Panels for Building Insulation, Energy and Buildings (in press 2014).

[12] Cabot Aerogel Particles Data Sheet: P100, P200, P300, P400, Boston, MA, 2013.

[13] W.P. Lewis (personal correspondence, January 31st, 2012).

[14] A. Basillais, S. Bensamoun, C. Chappard, B. Brunet-Imbault, G. Lemineur, B. Ilharreborde, M.-C. Ho Ba Tho, C.-L. Benhamou, Journal of Orthopaedic Science 12 (2007) 141.

[15] S. Brunauer, P.H. Emmett, E. Teller, Journal of the American Chemical Society 60 (1938) 309.

[16] E.P. Barrett, L.G. Joyner, P.P. Halenda, Journal of the American Chemical Society 73 (1951) 373.

[17] M.J. Assael, K.D. Antoniadis, W.A. Wakeham, International Journal of Thermophysics 31 (2010) 1051.

[18] M. Reim, G. Reichenauer, W. Körner, J. Manara, M. Arduini-Schuster, S. Korder, A. Beck, J. Fricke, Journal of Non-Crystalline Solids 350 (2004) 358.

[19] M. Reim, W. Körner, J. Manara, S. Korder, M. Arduini-Schuster, H.-P. Ebert, J. Fricke, Solar Energy 79 (2005) 131.

[20] E. Cohen and L. Glicksman, Analysis of Transient Hot-Wire Method to Measure Thermal Conductivity of Silica Aerogel, Influence of Wire Length, and Radiation Properties, ASME J of Heat Transfer 136 (2014) 041301.

[21] K.S.W. Sing, D.H. Everett, R.A.W. Haul, L. Moscou, R.A. Pierotti, J. Rouquerol, T. Siemieniewska, Pure and Applied Chemistry 57 (1985) 603.

[22] S.J. Gregg, K.S.W. Sing, Adsorption, Surface Area and Porosity, 1st ed., Academic Press, London, 1967.

[23] S. Jennings, Journal of Aerosol Science 19 (1988) 159.

[24] Y. Zuo, Preparation of Silica Aerogels with Improved Mechanical Properties and Extremely Low Thermal Conductivities Through Modified Sol-Gel Process, SM Thesis, Department of Mechanical Engineering, Massachusetts Institute of Technology, 2010.

[25] Cabot Aerogel: Aerogel for Insulation, Daylighting, Additives. *www.cabot-corp.com*. Retrieved March 17th, 2014, from http://www.cabot-corp.com/aerogel.

[26] Kurt J. Lesker Company Pressure Gauge Manual: 275i Series Convection Vacuum Gauge Module, Jefferson Hills, PA.

Table 1: Cabot granular aerogel compressive strain and corresponding bed density.

Compressive strain	Bed Density (kg/m^3)
0%	68
10%	76
20%	85
30%	97
40%	113
50%	136
60%	170
70%	227

Figure Captions

Figure 1: Micro-computed tomography images of compacted silica aerogels. (a) 10% compression, in air (b) Uncompressed, in water (c) 50% compression, in water and (d) 60% compression, in water. Note that in (a), in air, the granules are denser than air and are light gray while in (b), (c) and (d), the granules are less dense than water and are dark gray. Initial bed density ~68 kg/m^3. All images the same magnification.

Figure 2: Histograms of grayscale values of cross sections from micro-CT images of water/aerogel specimens compressed to (a) 10% and (b) 30% strain.

Figure 3a: Schematic of hot-wire test for compressed samples.

Figure 3b: Schematic of the vacuum chamber set-up for the hot-wire testing of aerogel granules.

Figure 4: Rebound strains at different times after release of 50% compressive strain.

Figure 5a: Rebound strains relative to original volume at multiple cycles of compression.

Figure 5b: Rebound strains relative to compressed volume at multiple cycles of compression.

Figure 6: Micro-computed tomography images of cross sections taken from water/aerogel samples at different levels of compression. All images at same magnification.

Figure 7a: The volume fraction of interstitial air between granules in the aerogel samples plotted against uniaxial compression strain. Initial bed density ~68 kg/m^3.

Figure 7b: Density of the granules calculated from the granular bed density and volume fraction of air at increasing compression strain.

Figure 8: Particle size distribution of granular aerogel at increasing compressive strain.

Figure 9: Particle size distribution of granular aerogel after compressive cycling to 50% strain, 1, 5 and 10 times.

Figure 10a: Plot of adsorption and desorption isotherms of the compressed granules.

Figure 10b: Plot of adsorption and desorption isotherms of granules compressed to 0, 40 and 70% strain. Data for other levels of compression similar (not shown for clarity of presentation).

Figure 10c: Cumulative distribution of pore sizes within the aerogel granules, for varying compressive strains.

Figure 10d: Pore characterization for one uncompressed sample, one sample compressed to 40% strain and one sample compressed to 70% strain. Each sample was tested three times.

Figure 10e: Pore characterization of the compressed granules. Three specimens were tested at each compression level; each specimen was tested once.

Figure 11: Thermal conductivity of granular silica aerogel from hot-wire testing at ambient pressure.

Figure 12: Thermal conductivity of granular silica aerogel from hot-wire testing under vacuum.

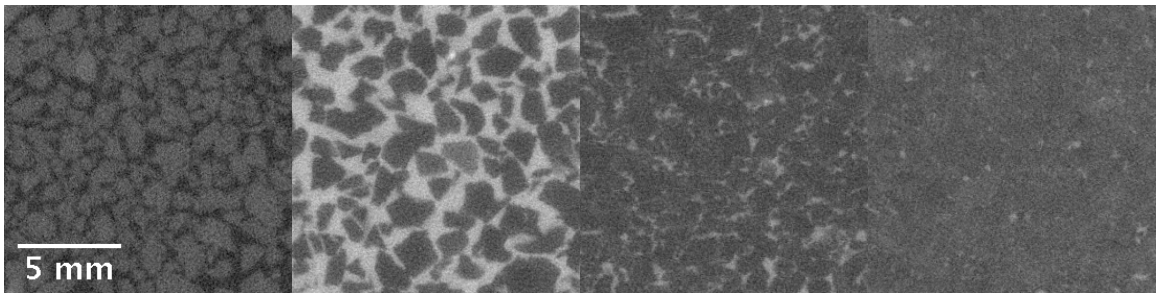

(a) (b) (c) (d)

Figure 1: Micro-computed tomography images of compacted silica aerogels. (a) 10% compression, in air (b) Uncompressed, in water (c) 50% compression, in water and (d) 60% compression, in water. Note that in (a), in air, the granules are denser than air and are light gray while in (b), (c) and (d), the granules are less dense than water and are dark gray. Initial bed density ~68 kg/m^3. All images the same magnification.

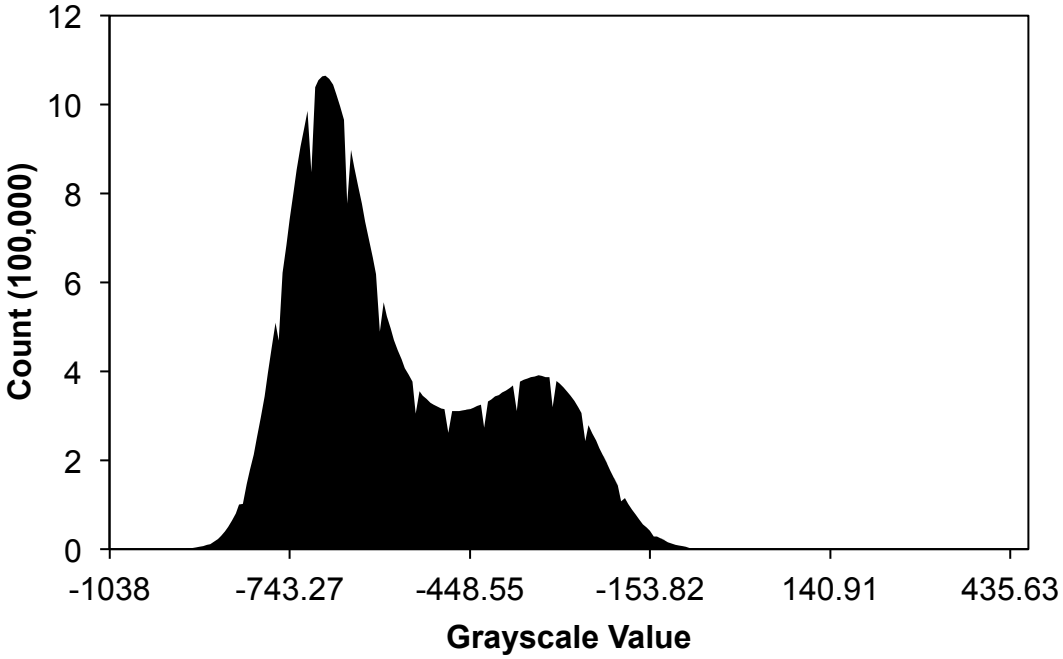

(a)

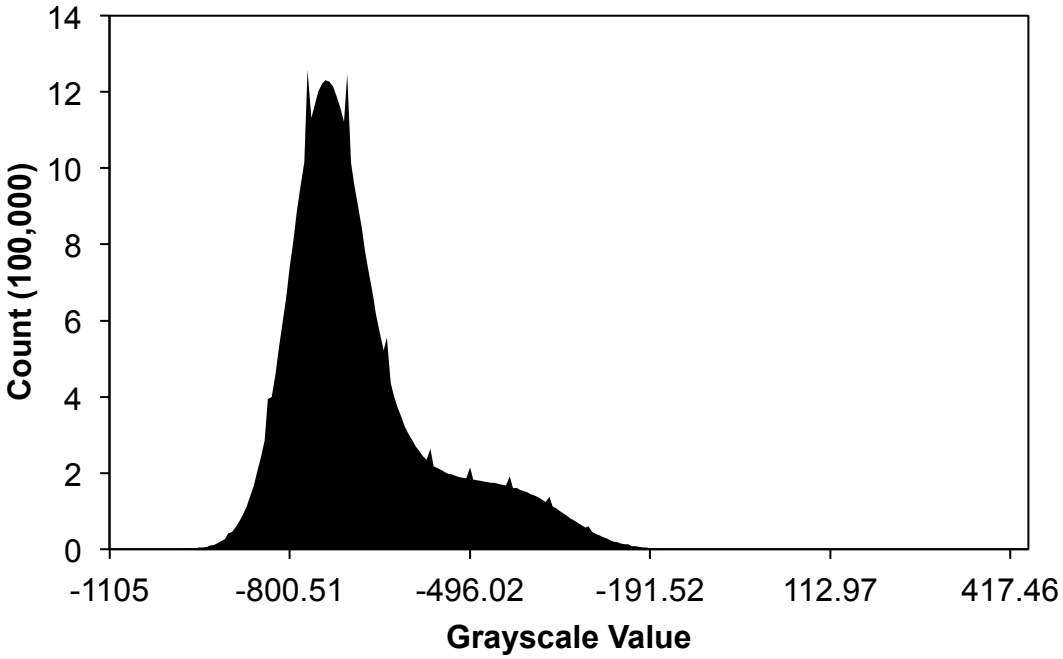

(b)

Figure 2: Histograms of grayscale values of cross sections from micro-CT images of water/aerogel specimens compressed to (a) 10% and (b) 30% strain.

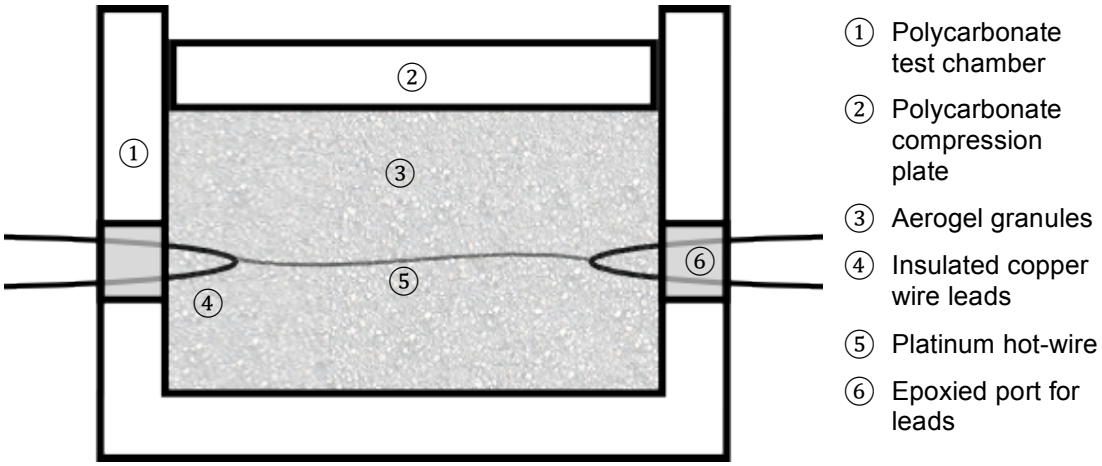

Figure 3a: Schematic of hot-wire test for compressed samples.

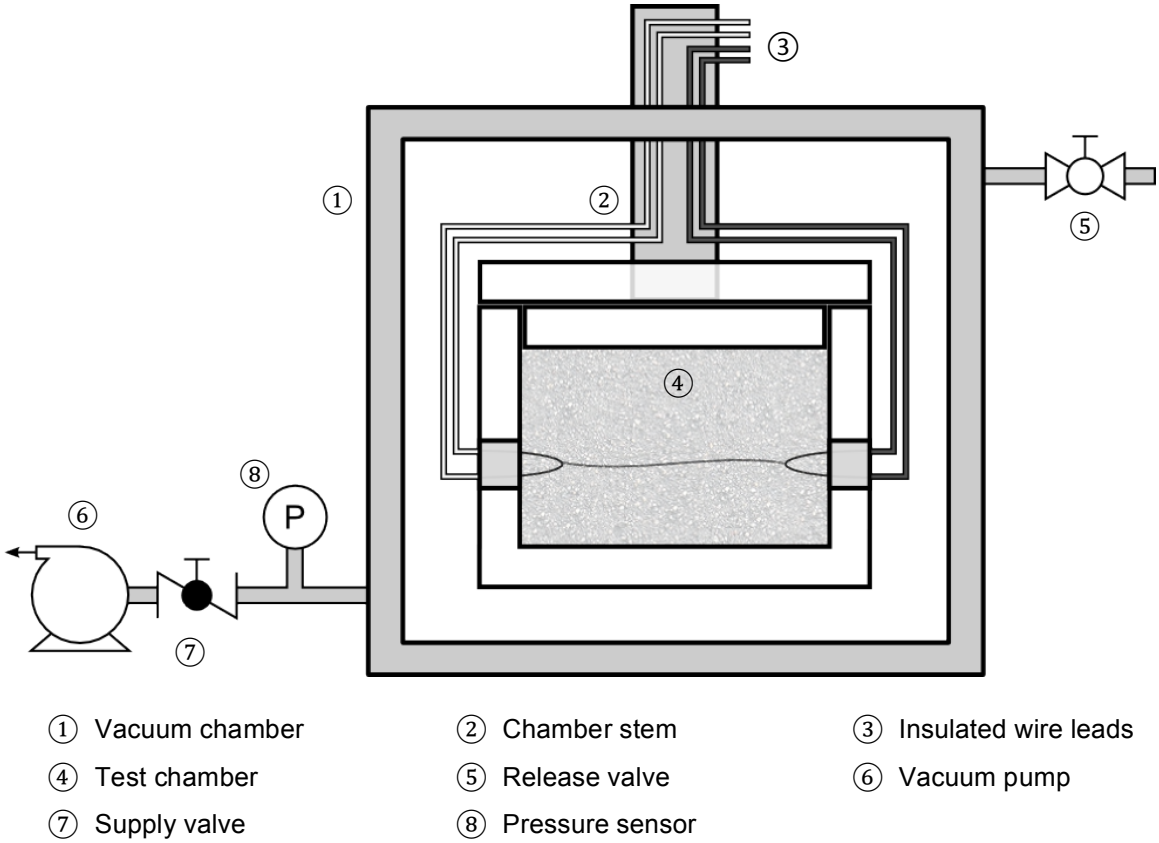

Fig. 3b: Schematic of the vacuum chamber set-up for the hot-wire testing of aerogel granules.

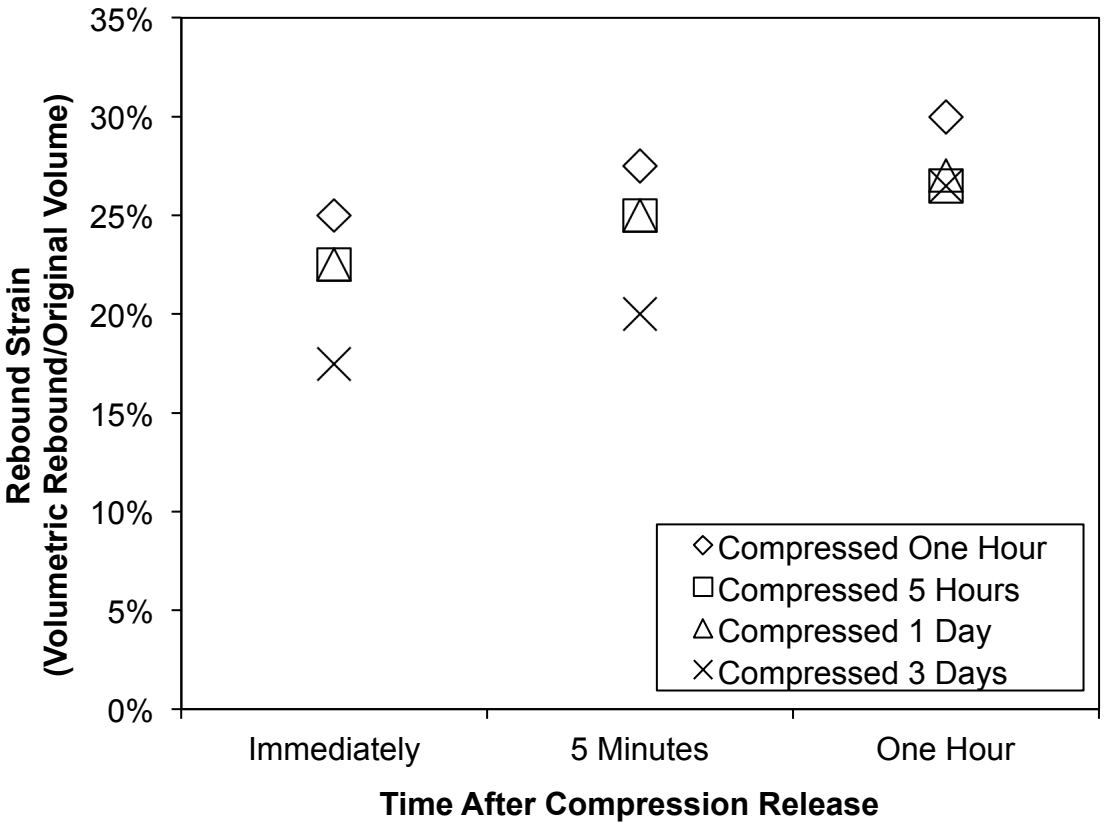

Figure 4: Rebound strains at different times after release of 50% compressive strain.

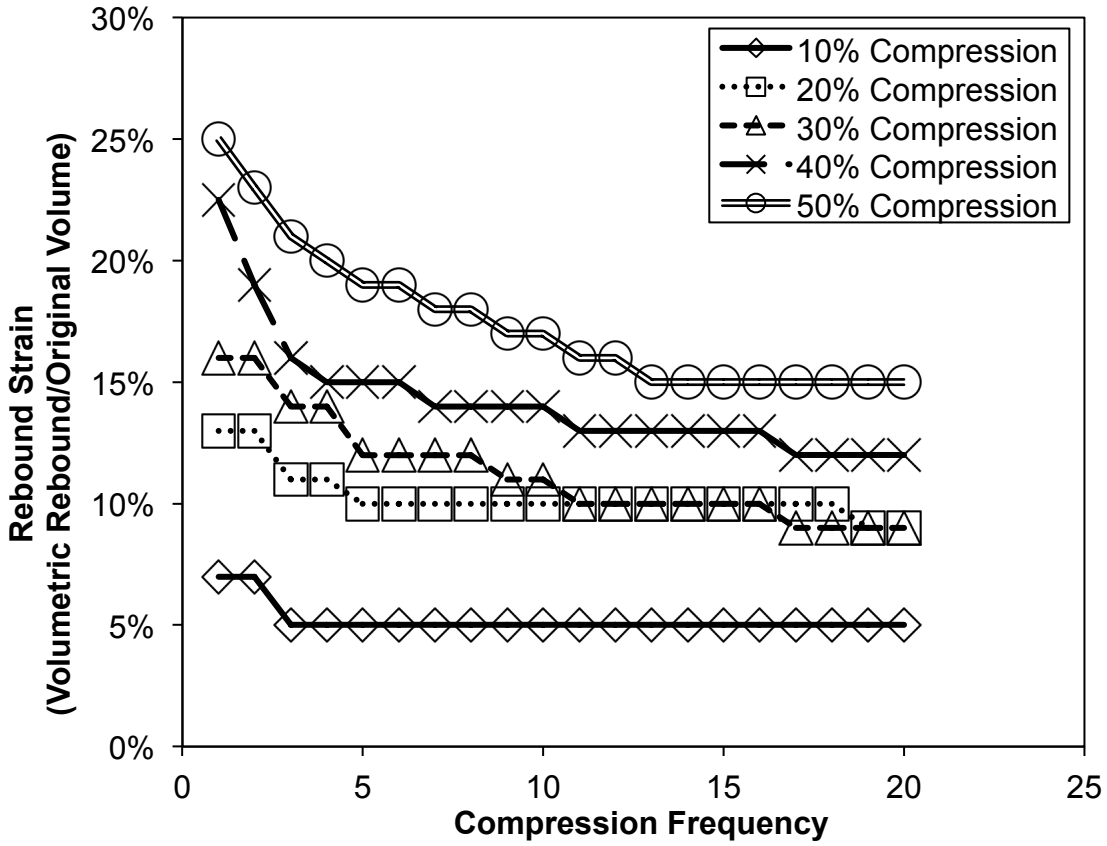

Figure 5a: Rebound strains relative to original volume at multiple cycles of compression.

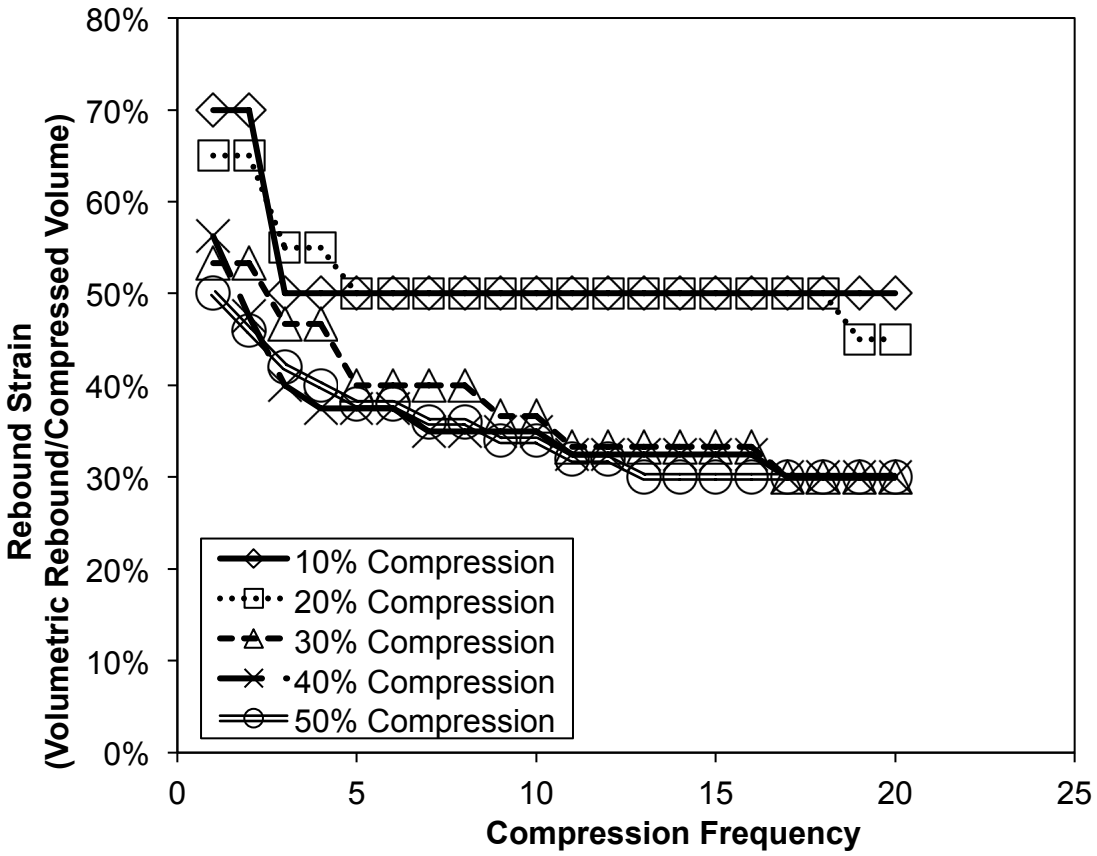

Figure 5b: Rebound strains relative to compressed volume at multiple cycles of compression.

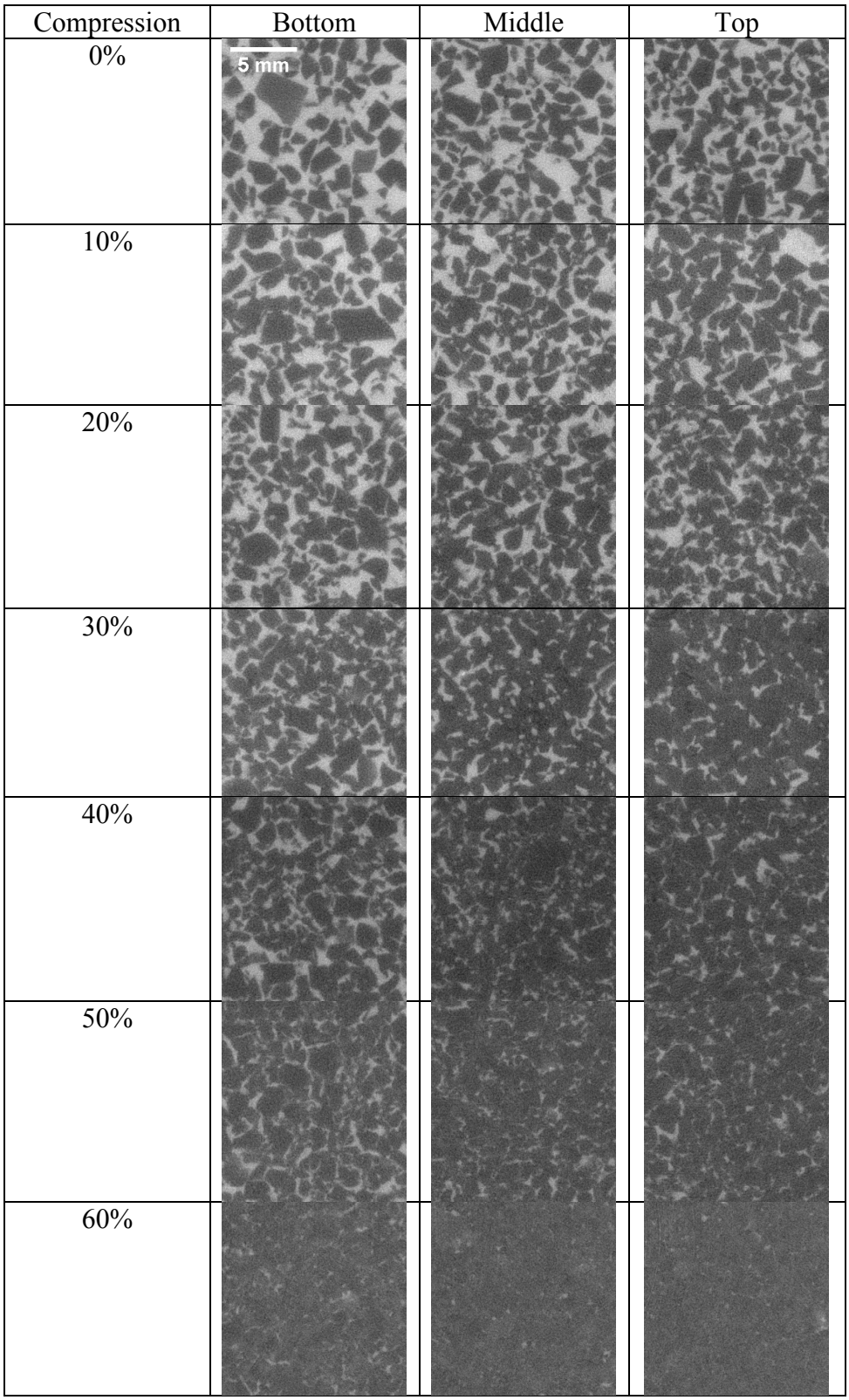

Figure 6: Micro-computed tomography images of cross sections taken from water/aerogel samples at different levels of compression. All images at same magnification.

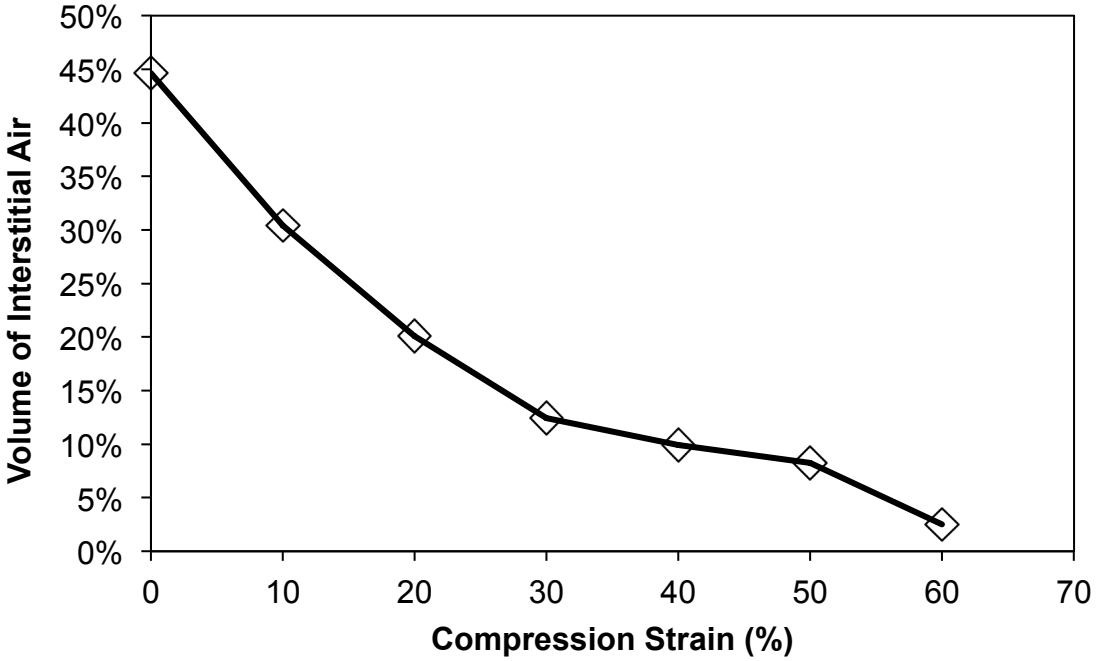

Figure 7a: The volume fraction of interstitial air between granules in the aerogel samples plotted against uniaxial compression strain. Initial bed density ~68 kg/m^3.

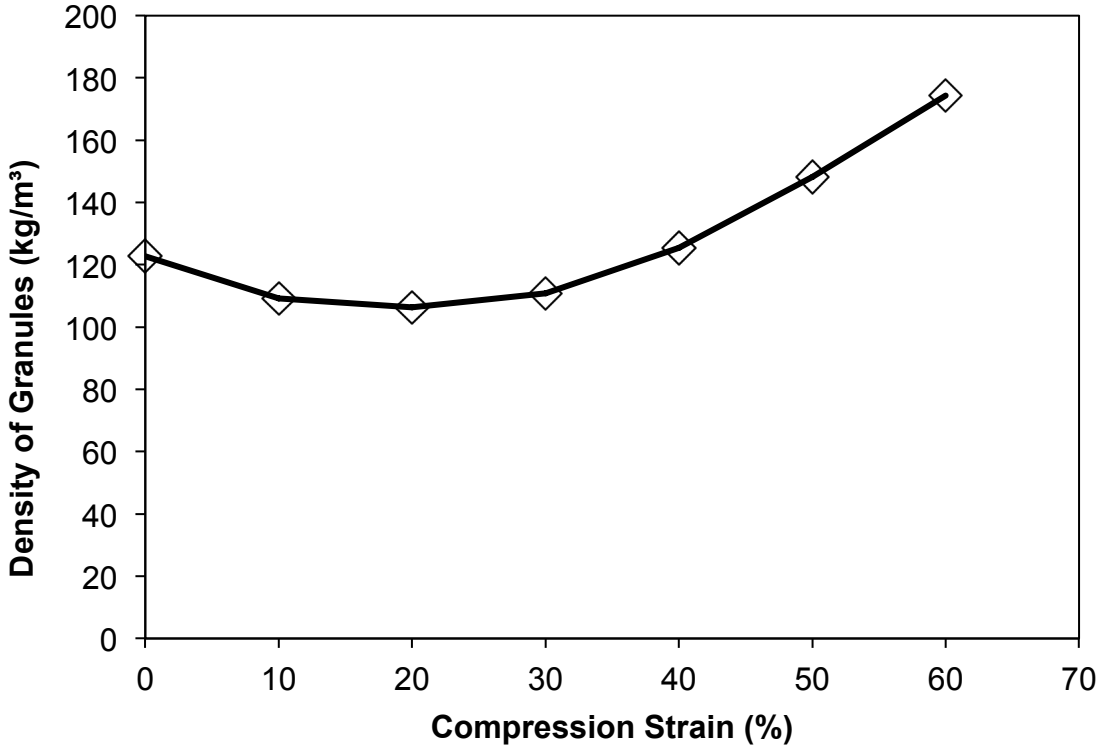

Figure 7b: Density of the granules calculated from the granular bed density and volume fraction of air at increasing compression strain.

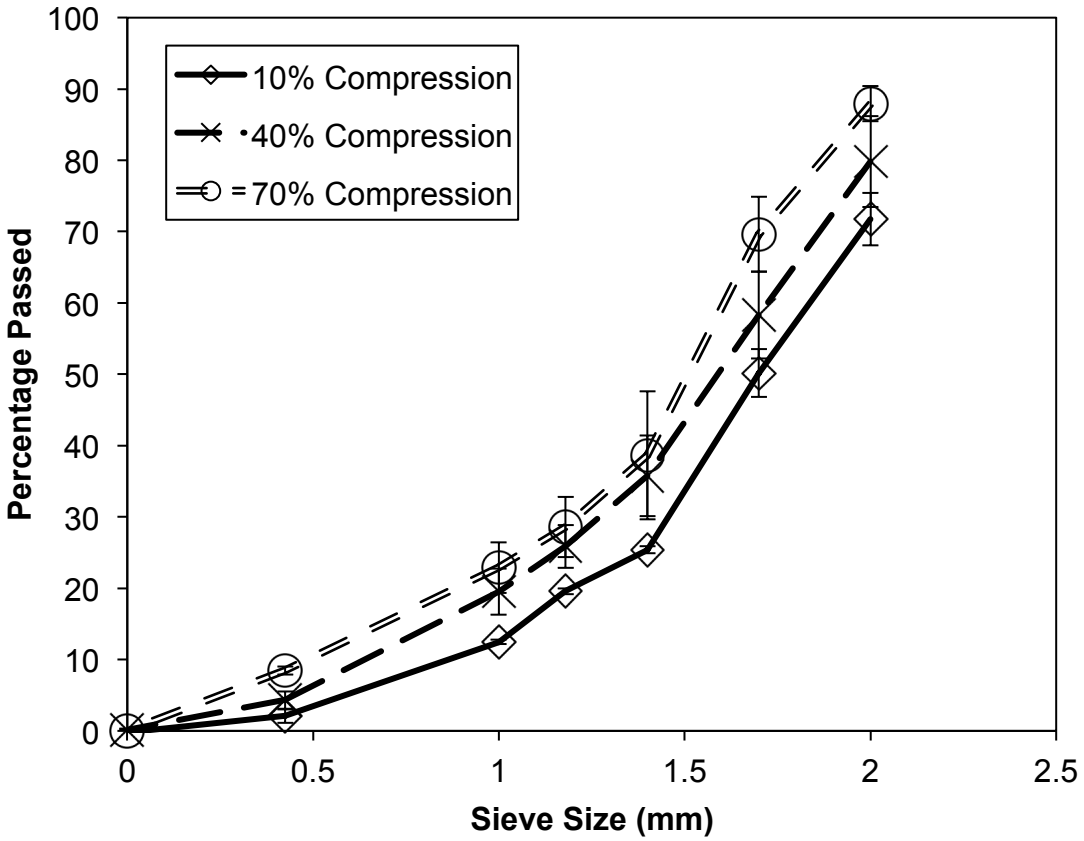

Figure 8: Particle size distribution of granular aerogel at increasing compressive strain.

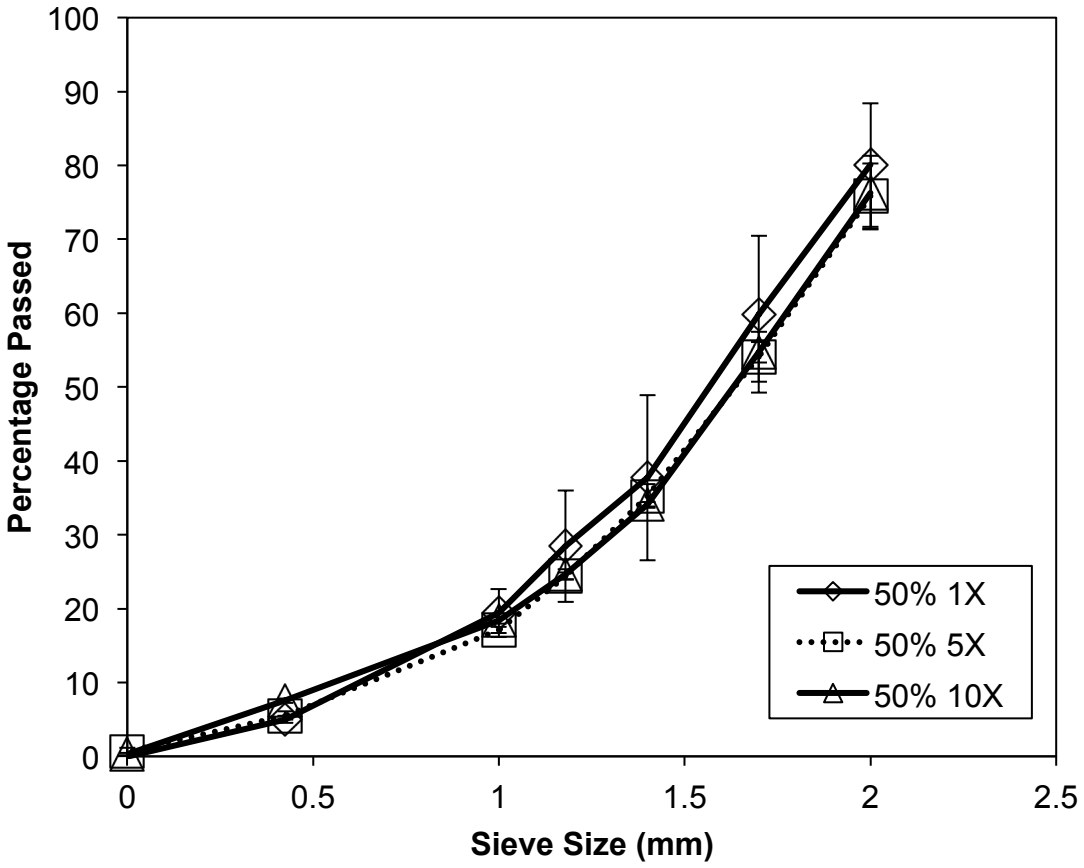

Figure 9: Particle size distribution of granular aerogel after compressive cycling to 50% strain, 1, 5 and 10 times.

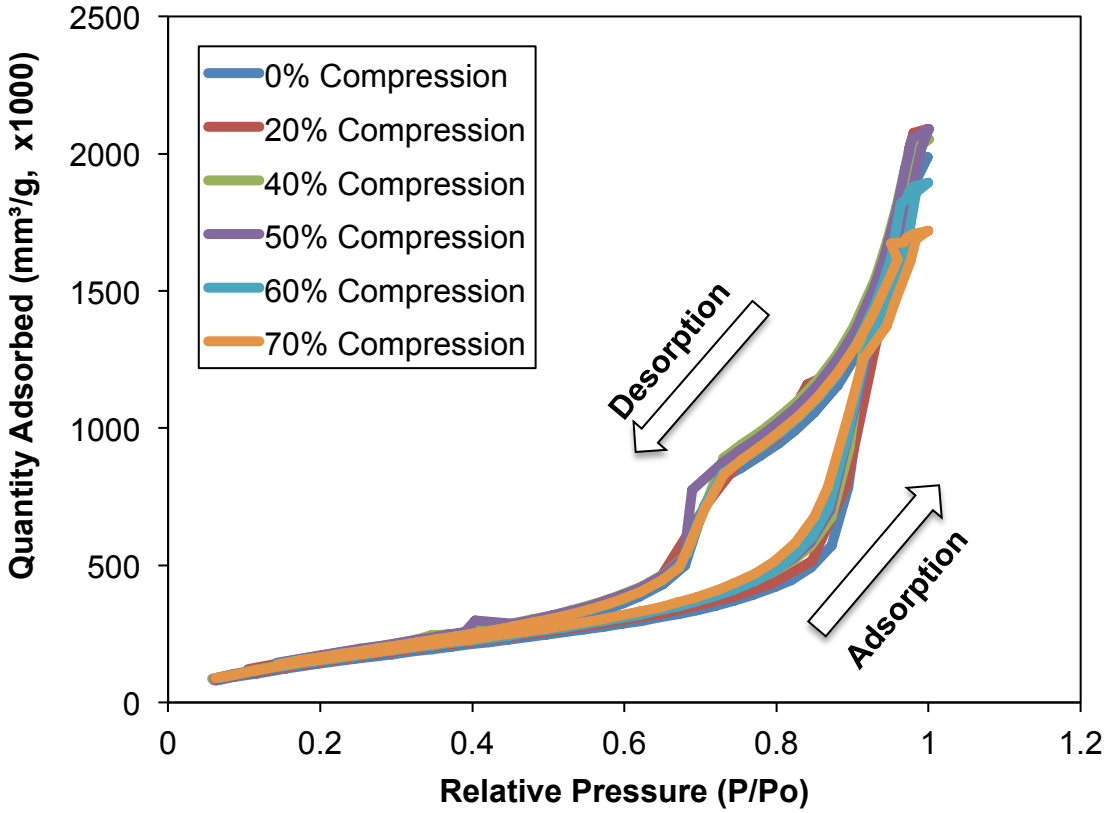

Figure 10a: Plot of adsorption and desorption isotherms of the compressed granules.

Figure intended for color reproduction on the Web and in print.

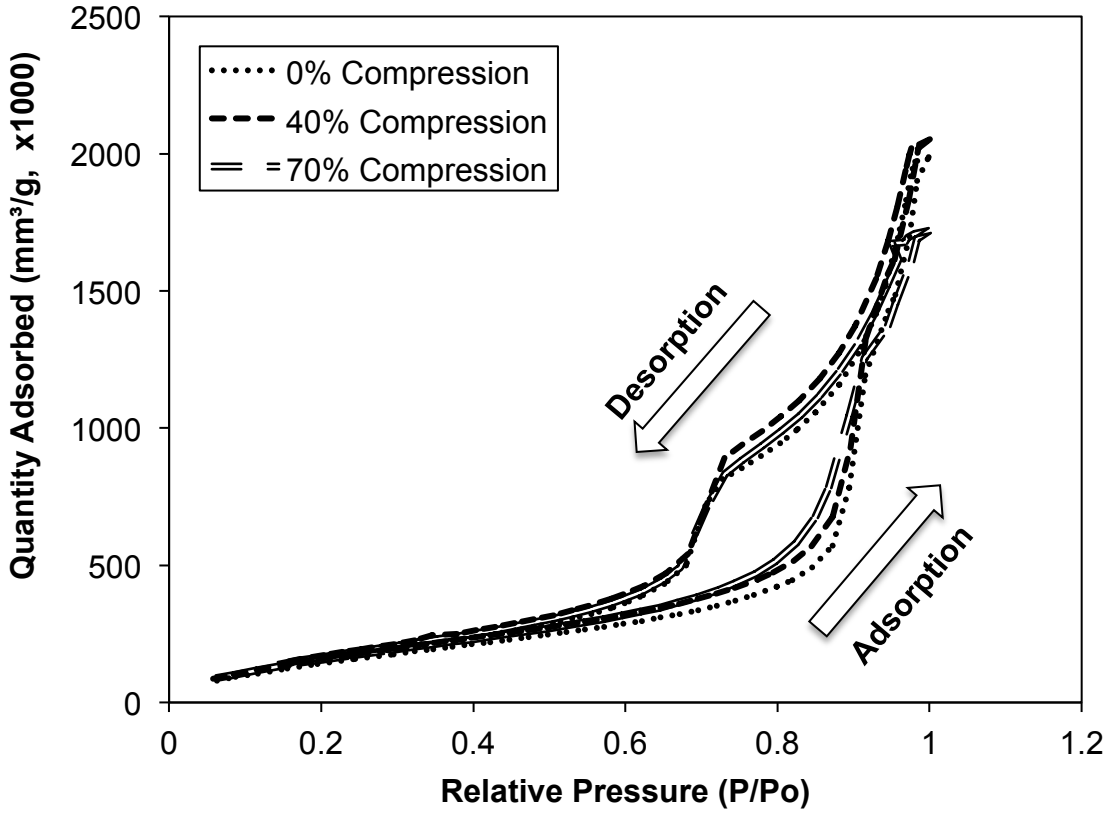

Figure 10b: Plot of adsorption and desorption isotherms of granules compressed to 0, 40 and 70% strain. Data for other levels of compression similar (not shown for clarity of presentation).

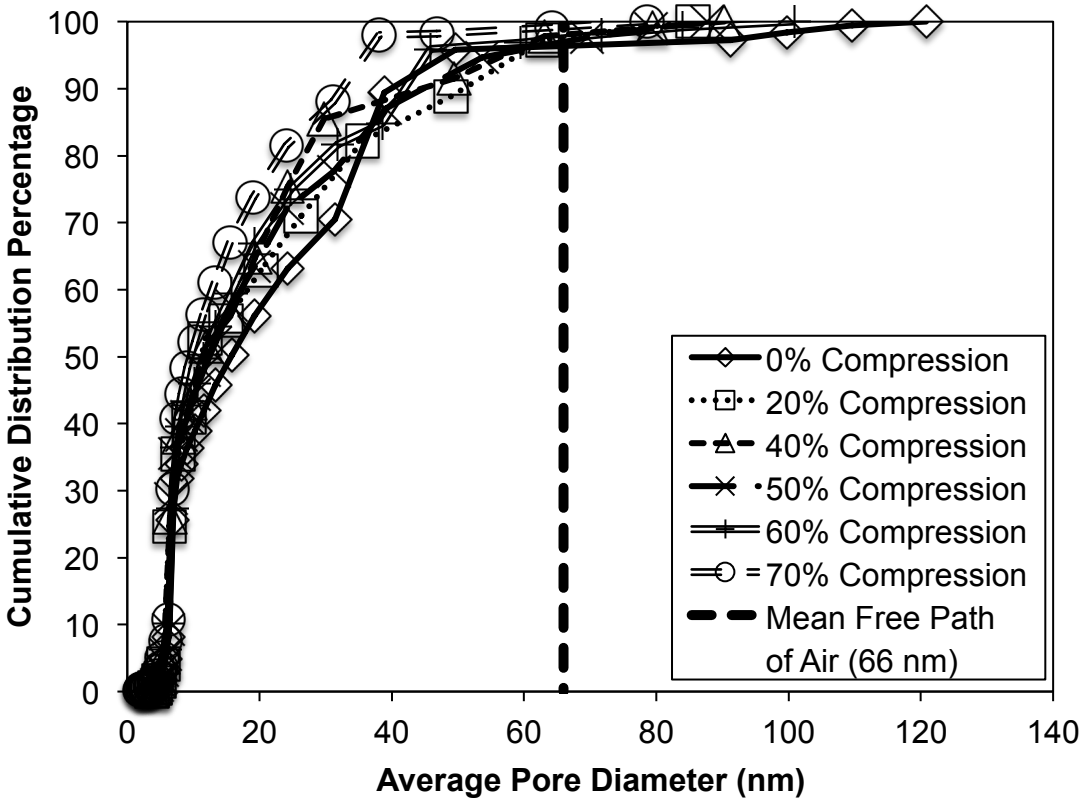

Figure 10c: Cumulative distribution of pore sizes within the aerogel granules, for varying compressive strains.

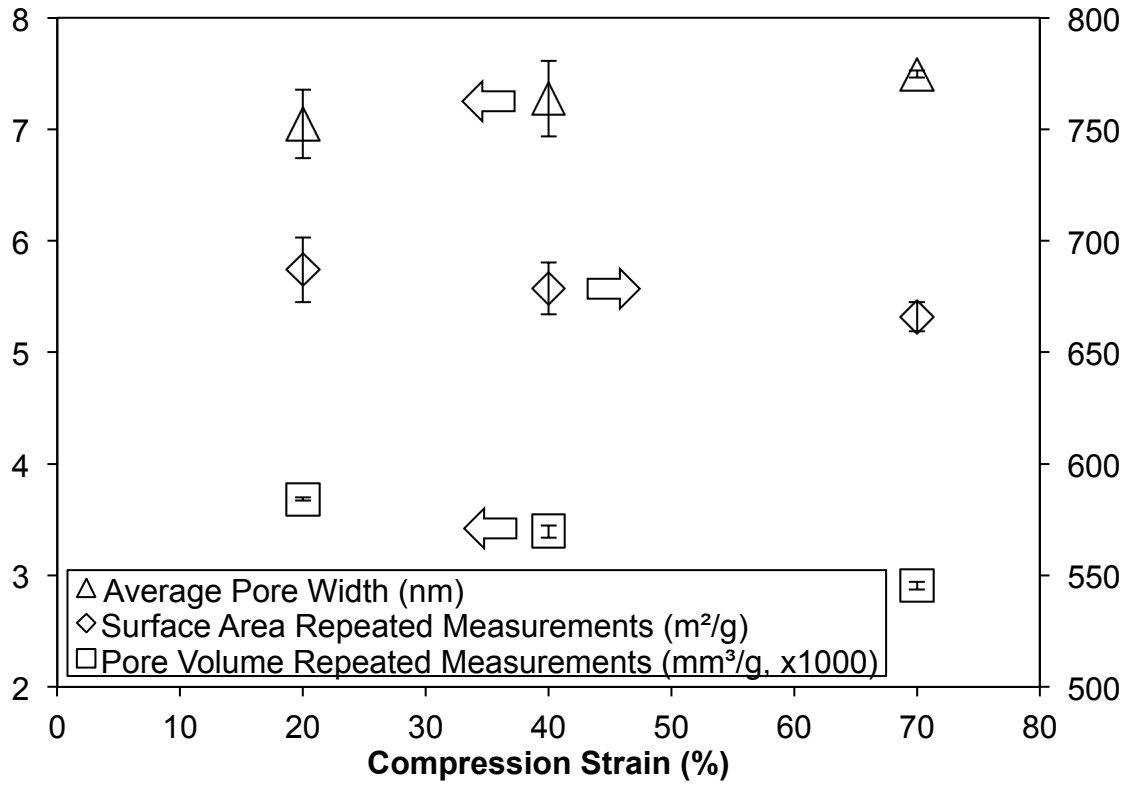

Figure 10d: Pore characterization for one uncompressed sample, one sample compressed to 40% strain and one sample compressed to 70% strain. Each sample was tested three times.

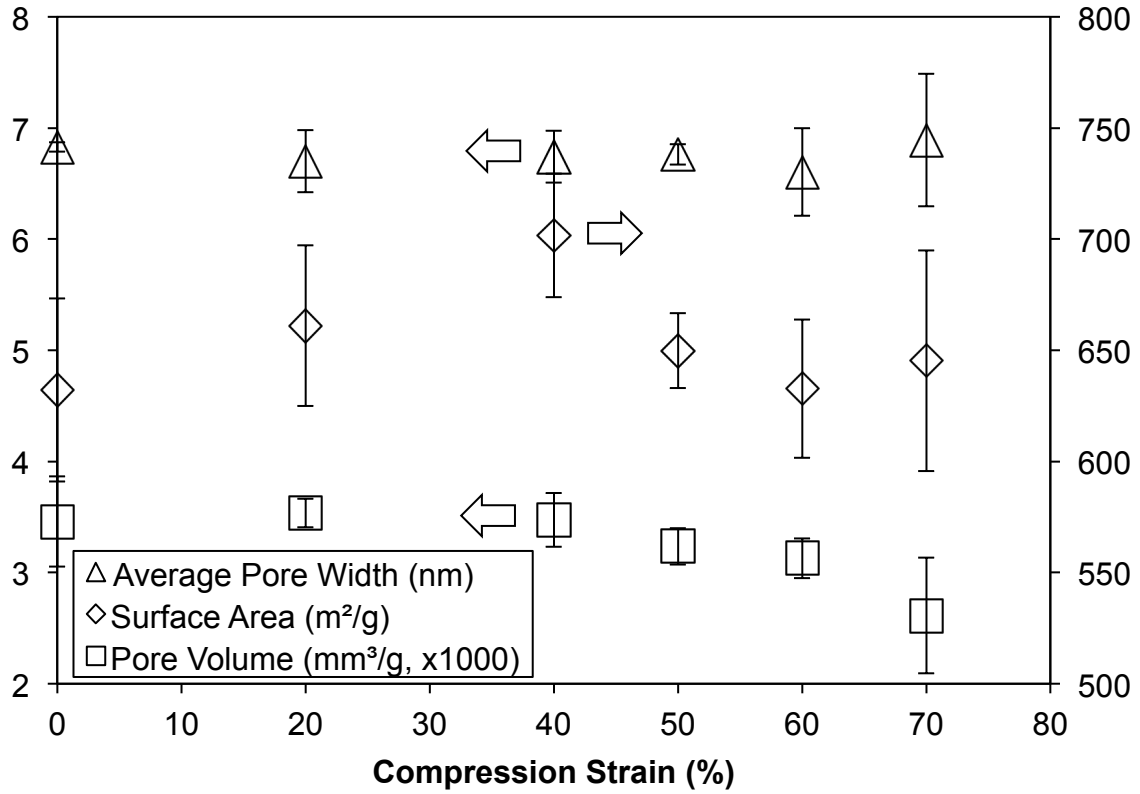

Figure 10e: Pore characterization of the compressed granules. Three specimens were tested at each compression level; each specimen was tested once.

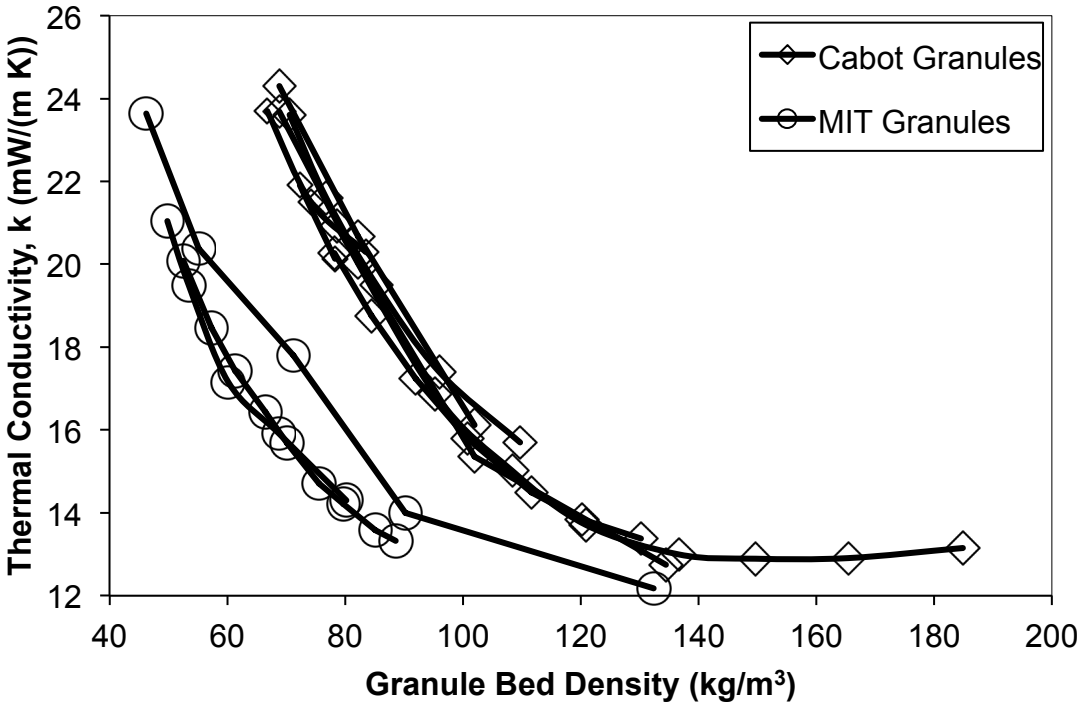

Figure 11: Thermal conductivity of granular silica aerogel from hot-wire testing at ambient pressure.

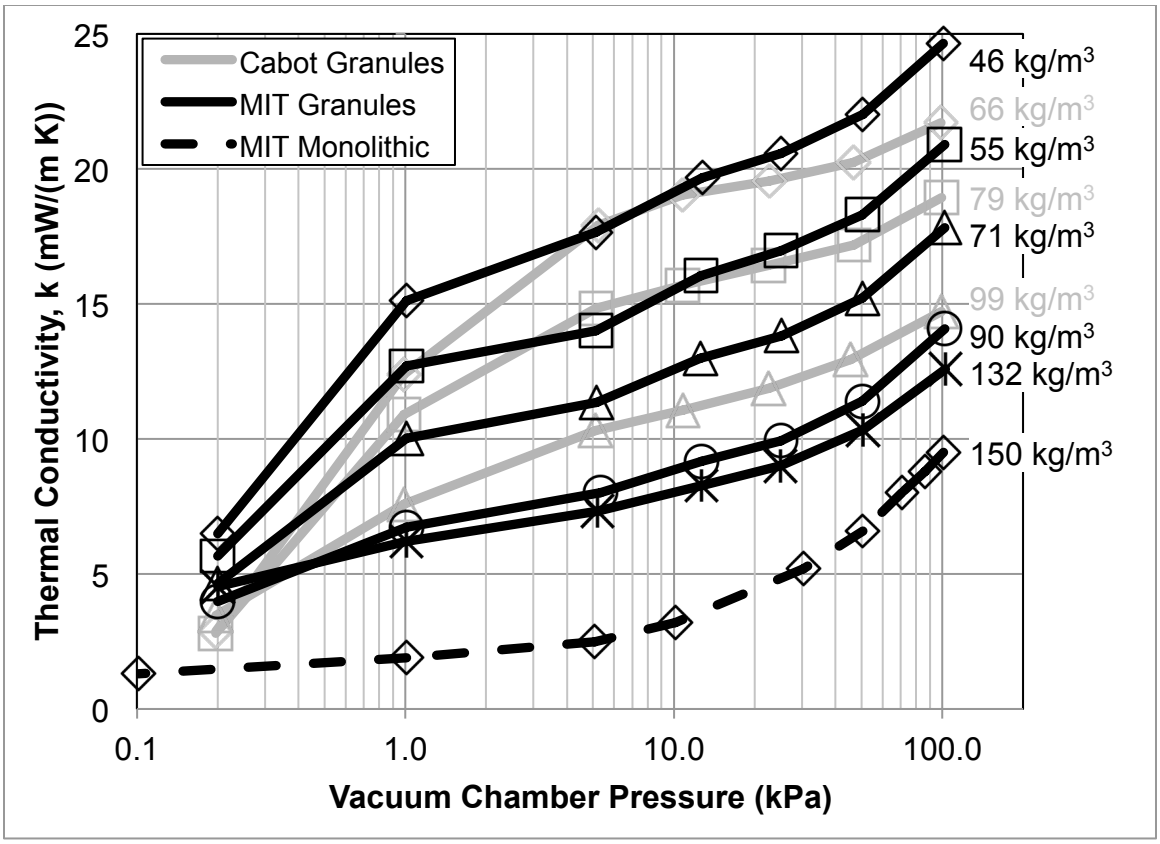

Figure 12: Thermal conductivity of granular silica aerogel from hot-wire testing under vacuum. Bed or monolithic densities are listed for each sample.